Mimicking 3D food microstructure using limited statistical information from 2D cross-sectional image

Antonio Derossi[a,*], Kirill M. Gerke[b,c,d,e,f], Marina V. Karsanina[b,c,d], Bart Nicolai[g,h], Pieter Verboven[g], Carla Severini[a]

[a] Department of Science of Agriculture, Food and Environment, University of Foggia, Italy
[b] Institute of Geospheres Dynamics of Russian Academy of Science, Moscow, Russia
[c] Schmidt's Institute of Physics of the Earth of Russian Academy of Sciences, Moscow, Russia
[d] Dokuchaev Soil Science Institute of Russian Academy of Sciences, Moscow, Russia
[e] Kazan Federal University, Kazan, Russia
[f] Moscow Institute of Physics and Technology, Dolgoprudny, Russia
[g] KU Leuven – University of Leuven, Division MeBios – Postharvest Group, Leuven, Belgium
[h] Flanders Centre of Postharvest Technology (VBCT), Leuven, Belgium

ARTICLE INFO

ABSTRACT

We used statistical correlation functions (CFs) to describe food microstructure and to reconstruct their 3D complexity by using limited information coming from single 2D microtomographic images. Apple fleshy parenchyma tissue and muffin crumb were chosen to test the ability of the reconstructions to mimic structural diversities. Several metrics based on morphological measures and cluster functions were utilized to analyze the fidelity of reconstructions. For the apple, reconstructions are accurate enough proving that lineal, L_2, and two-point, S_2, functions sufficiently describe the complexity of apple tissue. Muffin structure is isotropic but statistically inhomogeneous showing at least two different porosity domains which reduced the fidelity of reconstructions. Further improvement could be obtained by using more CFs as input data and by implementation of the techniques dealing with statistical non-stationarity. Novel stochastic reconstruction and CF-based characterization methods could improve the fidelity of reconstruction and future advances of this technology will allow estimating macroscopic food properties based on (limited) 2/3D input information.

1. Introduction

The need for characterization of 3D microstructure of food for understanding the role of 3D architecture in the sensorial and nutritional properties as well as in microbial growth has been reported recently by numerous authors (Aguilera, 2005; Parada and Aguilera, 2007; Datta, 2007; Takhar, 2016; Verboven et al., 2018). As the simplest digital structure model, the food may be considered as a two-phase (binary) system characterized by void (or pore) and solid material phases (Derossi et al., 2014). Several examples that may be described using such binary model include (but are not limited to) fruit and vegetables, bread, roasted coffee, cakes, ice-cream, cheese, chocolate, etc. In addition, their complex macroscopic properties such as texture, heat and mass transfer, gas diffusion, microbial growth and chemical reaction in restricted mobility conditions, as well as sensorial features, cannot be precisely explained and predicted without considering the nature of food as complex 3D structures. So, the possibility to estimate these properties from microscopic information, as well as their dynamics during processing and storage would have a definite impact in many practical applications. For instance, it is now acknowledged that for fruit and vegetables the diffusivity of gases in 3D structure of parenchyma tissue is a key factor for maintaining cellular metabolism. This, in turn, affects the evolution of fruit quality during storage (Verboven et al., 2008; Herremans et al., 2014). Hafsa et al. (2014) studied the three-dimensional properties of food agglomerates to improve the understanding of the relationships between wheat powders behavior during processing and the food products structure. Reinke et al. (2016), who studied the microstructure of chocolate, proved that the presence of cracks and voids created during processing may increase the well known problem of chocolate blooming, because they could act as channels for the migration of lipids. Datta (2007) study showed that the pore connectivity of food, which is of great importance

---

in food processing involving mass transfer, is tightly related with its intrinsic permeability k. Parada and Aguilera (2007) highlighted the importance of food microstructure on the bioavailability of several nutrients. In short, structural information is of utmost importance to assess macroscopic food properties numerically and to uncover the relationships between these properties (such as taste, diffusivity, storage capacity, etc.) and food's structure. Moreover, possible structural and temporal variability of the structure cannot be studied without imaging food samples.

Recent advances in imaging techniques, such as X-ray microtomography (XCT), magnetic resonance imaging, and laser scanning confocal microscopy, have provided a useful way for obtaining 3D information of food structure at various scales. However, these techniques do not completely address the problem of the quantitative and qualitative characterization of microstructure. More specifically, the commonly employed quantities to describe food microstructure, such as porosity and material fractions, mean cell size, fractal dimension, connectivity, size distributions of voids and material elements (Hafsa et al., 2014; Herremans et al., 2015a) furnish only a partial amount of the information necessary to accurately describe the complexity of 3D food structure, or are enough to assess only a limited number of important macroscopic properties. To accurately characterize any microstructure, the universal spatial correlation functions (CFs) are known to be very useful mathematical descriptors suitable for binary heterogeneous systems (Torquato, 2002). Several CFs containing different information about the structure at hand were proposed: the *two-point probability function*, S_2; the *lineal-path distribution function*, $L(r)$; the *pore-size distribution function*, $p(r)$; the *chord-length distribution function*, $p(r)$; and the *two-point cluster function*, C_2, to name a few (Smith and Torquato, 1988; Lu and Torquato, 1992; Torquato and Lu, 1993; Torquato, 2002). Historically, CFs have been widely employed in material science (Rintoul et al., 1996a,b; Chan and Govindaraju, 2004; Sheidaei et al., 2013; Guo et al., 2014) and digital rock petroleum engineering applications (Manwart et al., 2000; Talukdar et al., 2002; Yin and Zhao, 2014; Gerke et al., 2015) but later on established their way into soil science (Gerke et al., 2012; Karsanina et al., 2015), and, eventually, food science (Derossi et al., 2013, 2014, 2016).

It is well established that any digital structure can be fully characterized by *n*-point correlation functions, where *n* is basically the number of unique points (pixels/voxels) on the image of the structure (Torquato, 2002). In practice, it is desirable to describe the structure with as little number of descriptors as possible; in other words, utilize a minimum number of different low-order CFs. Moreover, it was shown that higher order correlation functions with $n > 2$ add only very limited additional information (Yao et al., 1993; Jiao et al., 2009). Using information theory concepts it was also shown that, depending on the microstructure complexity, a very limited number of CFs can be enough to get a complete characterization (Gommes et al., 2012). The most straightforward way to check if some structure at hand can be fully described by a given set of correlation functions is to solve the inverse problem – reconstruct the structure from the set of CFs. The very first stochastic reconstruction technique was based on a Gaussian random field (Quiblier, 1984; Adler et al., 1990). But as this approach is only limited to the use of a two-point probability function, a more universal approach suitable for any superposition of CFs and based on simulated annealing (Kirkpatrick et al., 1983) was proposed and is known as the Yeong-Torquato (Y-T) method (Yeong and Torquato, 1998a, 1998b). The method consists in an annealing procedure which analyzes the different states of a system starting from a random configuration and evolving it towards ground state (having a minimum energy) with correlation functions as close as possible to the reference system that we are attempting to reconstruct, i.e. original apple tissue and muffin structure in our case.

The comparison between the original representative volume element (REV) and the reconstruction allows to analyze the ability of different CFs to capture the essential microstructure properties of the system under study. Furthermore, reconstruction of 3D microstructure from 2D sectional images is of great important since obtaining 3D images (e.g. by means of µCT methodology) is expensive and time consuming. Also, obtaining accurate 3D pore space images is only possible if the pore sizes are larger than the imaging resolution. When 3D imaging methods fail or are not readily available, the reconstruction of 3D structure from 2D statistical information obtained from micrograph (e.g., SEM and FIB/BIB-SEM, including cryo-methods to preserve soft matter structure) images is a very attractive solution. Moreover, for hierarchical structures, i.e. where structural features such as pores, span over several imaging scales, a single methodology to study structure will either have insufficient imaging resolution or field of view. The only way to solve this conundrum is to employ multiscale image fusion (Gerke et al., 2015), which was recently successfully applied to a number of different pore containing systems (Gerke et al., 2017; Karsanina et al., 2018).

The Y-T technique and its modifications has been widely implemented to reconstruct several heterogeneous systems such as digitized model system (Rintoul and Torquato, 1997; Gerke et al., 2014), gels (Rintoul et al., 1996a,b), sandstones (Coker et al., 1996; Manwart et al., 2000; Yin and Zhao, 2014), galaxies (Jiao et al., 2009), shale rock (Gerke et al., 2015), stainless steel containing filamentary ferrite (Guo et al., 2014), pellets of α-alumina (Capek et al., 2009), soil (Karsanina et al., 2015), and bi-continuous composite (Li et al., 2016). In a previous paper we analyzed the possibility to implement the Y-T method to reconstruct representative 2D images of bread structure by using the only information contained in the lineal-path distribution function (Derossi et al., 2014). To the best of our knowledge, apart from this paper, reconstruction methods of food microstructure lack in literature. In particular, only Abera et al. (2014) tried to obtain a virtual generation of fruit tissue by statistical information while 3D stochastic reconstruction of food by means of universal correlation functions microstructure was never attempted previously.

All aforementioned microstructure characterization issues motivated current study. The aim of our work was to answer an important question regarding food structure characterization: can a conventional set of low-order correlation functions (preferably computed from one only 2D cross-sectional image) fully characterize a variety of food microstructures?

To address this question, for the first time, we have implemented the stochastic reconstruction procedure to reconstruct 3D microstructure of food from limited statistical information obtained from 2D cross sectional images of two types of food: 1) apple parenchyma tissue, and 2) muffin crumb. Also, we have examined the ability of a set of directional correlation functions to accurately describe the microstructure of samples by comparing original and reconstructed 3D image of food. Finally, we discuss all major advantages of correlation functions and current pitfalls of stochastic reconstruction technology and outline future steps to establish CFs as a routine approach to characterize food microstructure.

2. Material and methods

2.1. Food samples and image acquisition

As objects of our study we choose two food samples of very different genesis: 1) parenchyma tissue of the fleshy part of an apple, and 2) crumb from muffin as highly porous cereal-based food. The choice was motivated by a huge difference in microstructure of these two materials which, as we shall see later, enabled testing characterization approach using spatial CFs from diverse angles.

For the apple fruit samples, fruits of the cultivar Braeburn were harvested from orchards in Belgium at optimal picking dates in October 2014 and transported to KU Leuven. Fruit were stored in controlled atmosphere conditions until the time of X-ray imaging in January 2015. Conditions were 1 °C, 2.5% O_2, < 0.8% CO_2 according to the
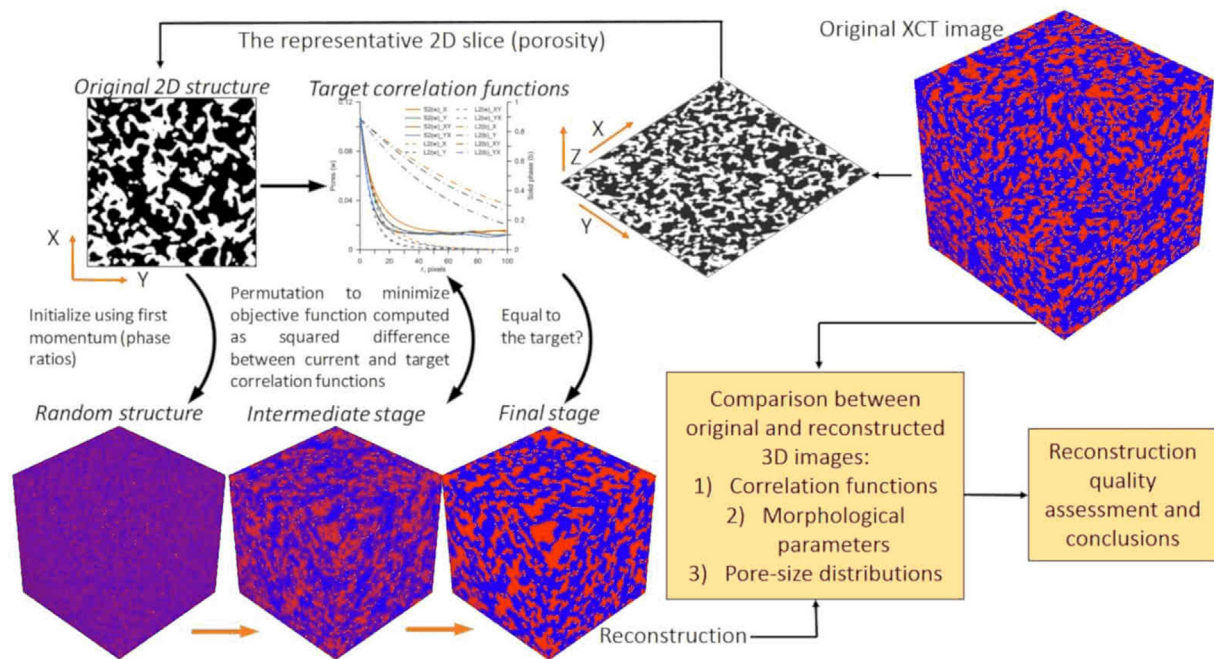
Fig. 1. The general scheme of the study, including image processing, 2D- > 3D image reconstructions and their verifications by comparison against original XCT images.

recommendations of the Flanders Centre of Postharvest Technology (www.vcbt.be). X-ray computed tomography was applied to visualize the porous microstructure of excised cylindrical apple cortex tissue samples according to the procedures of Herremans et al. (2015a) using a Skyscan 1172 (Bruker-SkyScan, Belgium) scanner. This resulted in a stack of cross-sectional images of the parenchymous cortex at 5 mm below the peel on the apple's equator. The cross sectional slices perpendicular to the fruit radius consisted of 1600 (x) × 1600 (y) pixels with a pixel size of 4.9 μm.

Muffin samples were manually prepared in laboratory under experimental conditions reported by Severini et al. (2017). A subsample of cylindrical shape was obtained by cutting along the length of the sample by using a cork bore of 3 cm in diameter. Then the cylinder was cut longitudinally to obtain a height of 3 cm. Cross sectional images of 1300 (x) × 1300 (y) pixels were acquired with a resolution of 18.83 μm which was sufficient to accurately capture all major features of muffin microstructure. The following conditions were used to obtain shadow projections of the muffin's structure: exposure time of 2 s, average images of four for each step angle of 0.2°, the energy of the X-ray tube was 50 kV, which resulted in total scanning time of 2 h.

2.2. Image processing

Original XCT images represent grey-scale images where each voxel has the intensity depending on X-ray absorption within respective sample's subvolume. First, we crop a cubic region of interest from each stack of images for both apple and muffin samples, 700^3 and 800^3 voxels, respectively. This is needed for a variety of reasons: 1) to remove all border effects due to sample's shape and imaging procedure, 2) cubic subvolume is convenient for further processing, as it basically represents a 3D matrix of same dimension, 3) the size of 700-800^3 voxels is a good compromise between image representability and computational efforts needed for its processing. The second crucial step is image segmentation into two materials (or phases): pores and solids. In this work we utilize converging active contours segmentation method (Sheppard et al., 2004). This segmentation approach requires two threshold confidence intervals (e.g., grey scale values that are pores or material with a high degree of certainty) for each of the two phases

to be separated. All threshold confidence intervals were chosen manually based on grey-scale histogram and trial segmentation runs. In case of the apple grey scale 3D image, before segmentation we applied non-local means filter (Buades et al., 2005) to improve signal-to-noise ratio. All image processing was performed using in-house code developed by the FaT iMP research group (http://www.porenetwork.com).

2.3. Computation of CFs and stochastic reconstruction

To characterize microstructure and later on perform stochastic reconstruction we first compute a sets of directional correlation functions (Kumar et al., 2006; Jiao and Chawla, 2014; Gerke et al., 2014) for 2D and 3D images. In this study, three types of correlations functions were employed: 1) the two-point probability function S_2 describing the probability that two points separated by a vector displacement $r(x_1, x_2)$ between x_1 and x_2 lie in the same phase; 2) the linear function L_2 describing the probability that the whole segment r lies within the given phase; 3) cluster function C_2 describing the probability that x_1 and x_2 lie in the same cluster (a 6-neibhours connected conglomerate of void/pore voxels). Note that while S_2 and C_2 are computed for pore phase only, the linear correlation function is computed separately for both pore and material phases. There is no benefit in computing S_2 for both binary phases, as each one of them can be calculated from the other (Torquato, 2002). We calculate S_2 and L_2 in two or three orthogonal and two or six for diagonal directions, for 2D and 3D images respectively, which are then used separately during reconstruction (Gerke et al., 2014). The C_2 function is evaluated in three orthogonal directions for 3D images only, as connectedness information is fundamentally different in two and three dimensions (Lee and Torquato, 1988; Torquato, 2002; Čapek et al., 2009). All details of directional CFs computation were previously described in detail, thus only brief description was provided here, for more information we refer to Gerke et al. (2014) and Karsanina et al. (2015).

For any set of correlation functions considered in the 3D reconstruction technique, matching correlation functions of a given realization with an original reference structure is based on voxel permutations (see general scheme on Fig. 1). If a set of two-point correlation functions used in reconstruction is provided in the form of $f_2^\alpha(r)$, where

α is a type of correlation function and r is a segment of varying length, the difference between two realizations of the structure can be expressed as the sum of squared differences between sets of correlation functions (Yeong and Torquato, 1998a; Gerke and Karsanina, 2015; Derossi et al., 2016):

$$E = \sum_{\alpha} w_{\alpha} \sum_{r} \left[f_2^{\alpha}(r) - \hat{f}_2^{\alpha}(r) \right]^2, \tag{1}$$

where $f_2^{\alpha}(r)$ and $\hat{f}_2^{\alpha}(r)$ are the values of the correlation function sets for two realizations (where the former represents a reference food microstructure while the latter represents the food microstructure under reconstruction), w_{α} is a weight factor used to improve convergence. In Eq. (1), E represents the 'energy' of the system, which is minimized by the simulated annealing algorithm. We start from a random structure and change voxel positions, while checking the system's energy according to Eq. (1). The Metropolis algorithm is used (Metropolis et al., 1953) for the simulated annealing algorithm which describes the probability p of accepting (or rejecting) each single random permutation of pixels between void and material phases (the examples of random structure evolution are shown in Fig. 1 and in Fig. 1 in Derossi et al. (2014), very detailed reconstruction process workflow scheme is available in Fig. 2 in Karsanina et al. (2015)) – e.g. between a single couple of black and white pixels randomly choose and interchanged in 3D structure - in the following way:

$$p(E_{old} \rightarrow E_{new}) = \begin{cases} 1, & \Delta E < 0 \\ \exp\left(-\frac{\Delta E}{T}\right), & \Delta E \geq 0 \end{cases}, \tag{2}$$

where T is the so-called 'temperature' of the system, and

$$\Delta E = E_{new} - E_{old}. \tag{3}$$

The initial temperature T is chosen so that the probability p for $\Delta E \geq 0$ equals 0.5 (Yeong and Torquato, 1998a, 1998b). We utilized the following cooling schedule based on geometrical progression of the form:

$$T(k) = T(k-1)\lambda, \tag{4}$$

where k is the time step and λ is a parameter smaller than but close to unity. Note that k is simply a number of trial and error attempts of the optimization procedure and does not represent any physical time; also depending on the acceptance/refusal of the attempt the physical CPU time needed for each time step may be different (and, thus, assessed in bulk). We used the annealing schedule parameter $\lambda = 0.999999$ for all reconstructions.

To improve the speed of convergence, we adopted a relatively simple permutation approach following Čapek et al. (2011) and Vesely et al. (2015): 1) choosing a random location within a phase of interest, and 2) choosing two random directions in which two pairs of pixels with a minimum distance in-between are selected such that they satisfy the conditions of lying in opposite phases and at the interface. The size of all 3D reconstructions was 512^3 voxels, which is a good trade-off between the volume of the reconstruction and computational resources required. We chose cut off length of $r = 250$ for all CFs computations and stochastic reconstructions, which actually makes sense as this values is half of the reconstruction size. Periodic boundary conditions were applied for CFs evaluation during reconstruction procedure. Note, that only conventionally applied S_2 and L_2 (for both pore and material phases for linear function) correlation functions were utilized during reconstructions (the use of the cluster function will be explained later). This technically means that we reconstructed both void and material phases at the same time (recalling the fact that computing S_2 function for both phases is impractical as mentioned earlier). The reconstruction procedure was terminated after 10^6 consecutive unsuccessful permutations. Weight factors w_{α} were chosen according to the methodology described in Gerke and Karsanina (2015).

One more important methodological aspect requires thorough

explanation. Namely, how do we perform 3D image reconstruction from a 2D cross-section. At first, we need to choose such representative 2D image from the original 3D XCT image. This is done by subsequent computation of pore fraction within each 2D cross-section along the main direction of sample. The 2D image with porosity value closest to that of the whole 3D image is chosen as the most representative cross-section. The full set of directional S_2 and L_2 (both phases), 12 CFs in total, is computed for such 2D data used as input data for stochastic reconstructions. We start by a random mixture of pore and material voxels (Fig. 1). Note, that the phase ratio between pores and material is immediately known from the first momentum of any correlation function used, i.e., $S_2^{pores}(0) = L_2^{pores}(0) = 1 - L_2^{solids}(0)$. The third "unknown" dimension during reconstruction (which is not possible to be evaluated from the input 2D image) is deduced as average of the respective directional CFs on the 2D image. For example, S_2_Z is computed as an average of S_2_Y and S_2_X (see Fig. 1 for schematic explanation). This allows obtaining all CFs in three dimensions from a single 2D image. After reconstruction is obtained, the CFs in all dimensions are computed for both original and reconstructed images and compared to evaluate the accuracy of this procedure. After target CFs set is created using direct computations from input 2D image and extrapolating them into unknown 3rd dimension (assuming that the sample is almost isotropic), the random 3D voxel mixture is evolved by simulated annealing algorithm (Eqs. (2)–(4)) to the state where the different between target and current CFs is minimal. The resulting 3D image is the 3D stochastic reconstruction.

All four stochastic reconstructions performed for this study were successful in terms of simulated annealing procedure – energy according Eq. (1) was cooled down to a group state, i.e., $E \rightarrow 0$. In practice reaching exactly zero is too time consuming (Rozman and Utz, 2002) and impractical for large reconstructed images. For each food sample we have chosen two representative 2D images. Each such 2D cross-section was used as input data for stochastic reconstruction as described above with the volume of 512^3 voxels. In this way we created four 3D reconstructions, two for apple tissue and two for muffin. From now on these stochastic replicas will be referred to as Reconstruction 1 and Reconstruction 2 with either Apple or Muffin prefix.

2.4. Comparison of XCT and reconstructed 3D images using different metrics

To verify the accuracy of the resulting stochastic reconstructions we appeal to a wide variety of comparison metrics. First, we compare original XCT and resulting reconstructions visually by visualizing their microstructure. After such qualitative first check is performed, we employ quantitative metrics such as: 1) connectedness difference (defined below) computed with the help of C_2 cluster correlation function; 2) structure thickness, which indicates the diameter of largest sphere entirely bounded within the pore space (μm); 3) structure separation, defined in the same manner, but computed for the material phase (μm); 4) number of pores), 5) pore size distribution, i.e., the distribution of structure thickness parameter described above; 6) object surface/volume ratio (1/μm), indicating the ratio of material surface to volume measured within the volume of interest; 6) surface convexity index (1/μm). Except for the very first C_2-based metric all characteristics were computed using CTAn software (Bruker, SkyScan). The connectedness difference was computed from evaluated C_2 CFs according to:

$$Err_{C_2} = \frac{\sum_r \sum_d \left[C_2^d(r) - \hat{C}_2^d(r) \right]^2}{N(d)} \tag{5}$$

where $N(d) = 3$ is the number of directions for calculating the orthogonal cluster function, $C_2^d(r)$ and $\hat{C}_2^d(r)$ are the C_2 CFs for the original XCT and reconstructed microstructures, respectively. Computed in this way, Err_{C_2} is simply a difference in cluster correlation function
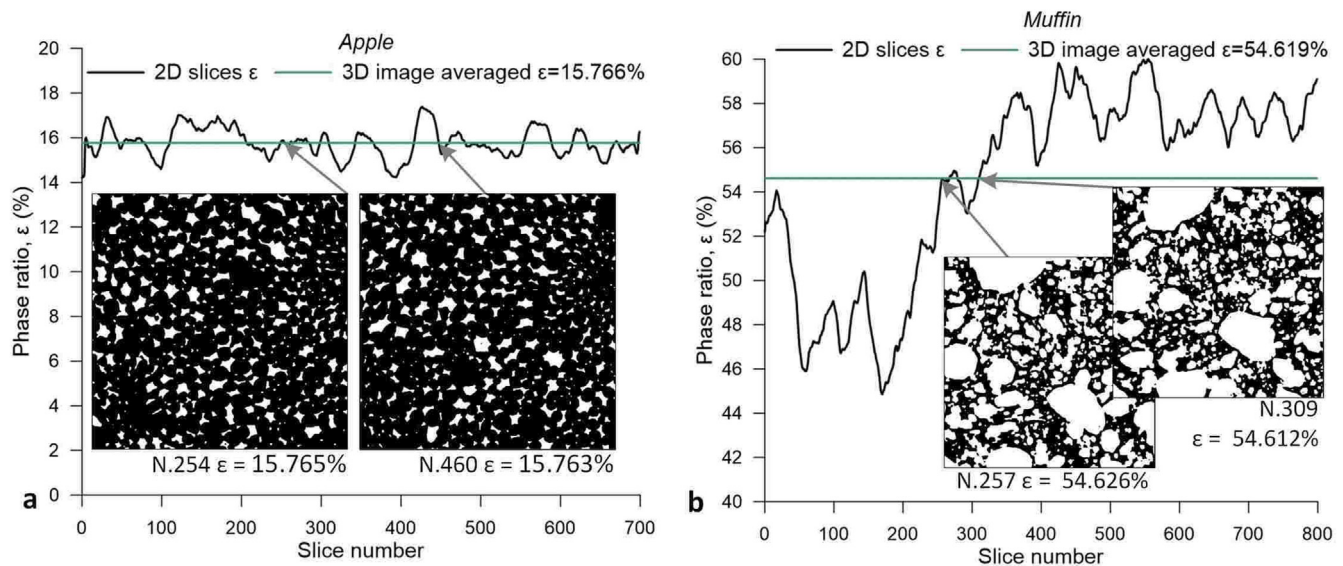
Fig. 2. Porosity analysis in binary cross-sectional images of a) apple and b) muffin samples. Two representative cross-sections for each sample later used for reconstructions are also inserted and their respective positions along Z-axis (slice number) are shown with grey arrows. Note that porosity values are scaled similarly for both graphs to highlight differences in variability between food samples.

according to Eq. (1).

After all aforementioned metrics are computed one can easily access the accuracy of the reconstructions by intercomparison of all computed values between original XCT image and its stochastically reconstructed 3D replicas.

3. Results and discussion

3.1. Microstructure characterization of apple tissue and muffin structure

The porosity fractions computed for all cross-sectional images of apple tissue are reported in Fig. 2a. The fluctuations between 14.36 and 17.54% well reflect the natural variability of fruit tissue structure. However, when of the whole XCT image of 700^3 voxels was analyzed, the overall porosity fraction of 15.77% was obtained. These results agree well with the data reported for Braeburn apples for which a porosity fraction between 15 and 19.9% was measured from XCT images (Herremans et al., 2014, 2015a). Also the figure shows two cross-sectional images chosen to compute the correlation functions employed as input data for stochastic reconstructions. Both slices (n.254 and n.460) showed porosity values of 15.76% exhibiting a relative difference from the whole XCT image below 1%.

Muffin samples showed a greater variability along Z-direction with the 2D micro-CT slices having porosity fraction between 45.03% and 60.2% (Fig. 1b). This is more than expected since the microstructure of muffins is subjected to many processing variables such as mixing conditions, rheological properties, expansion and water evaporation during baking, etc. Similarly, Van Dyck et al. (2014) who studied the changes in microstructure of bread structure reported significant variations in porosity across different regions of bread crumb. When the whole XCT image of 800^3 voxels was considered, a porosity fraction of 54.612% was computed while 2D cross-sectional slices (n.257 and n.309) employed to compute target CFs exhibited a porosity of about 54.62%, again, showing a relative difference below 1% (Fig. 2b).

Fig. 3 shows all CFs computed for binary XCT images of apple and muffin. The shape of correlation decay for all functions confirms that the cut-off $r = 250$ pixels (or ≈ 1.2 mm and ≈ 4.7 mm for apple and muffin, respectively) was enough to capture all important microstructure characteristics, including that of the solid phase ($L_2{}^b$). For simplicity of interpretation we did not show diagonal CFs – they behave more or less similar to orthogonal directions and substantially hamper

curve visibility.

We start with characterization of the apple microstructure (Fig. 3a). At first, we immediately notice that all correlation functions exhibit the same trend: X and Y directions agree almost perfectly, whilst the decay in Z-direction is slower indicating a somewhat more connected structure. This means that apple microstructure is not perfectly isotropic, as assumed in our stochastic reconstruction methodology, yet the degree of anisotropy is not significant. Second, as cluster functions reach zero values it means that void phase within apple sample does not percolate, i.e., it does not form a (single) well-connected cluster of pores within the sample and exhibits a certain level of separation formed by the material phase between individual pores. Moreover, C_2 decays similarly to L_2 function, which means that the connectivity is achieved only within a single pore element – all pores are separated by tissue cells, i.e., they do not agglomerate into clusters of pores connected via more narrow throats (Miao et al., 2017), as we later observe for muffin. According to the linear CFs the probability to find pores larger than $\sim 200\,\mu m$ in X and Y directions is very low with L_2 of 0.0006, while pores are more elongated in Z-direction with a non-zero probabilities up to a length of 350 μm. This indicates some variability of pore sizes and shapes along the radial direction of the fruit, and such differences were observed experimentally between the core, inner and outer cortex of apples (Verboven et al., 2013; Herremans et al., 2015b).

Based on similar considerations, in a previous paper we have quantified apple tissue by using statistical correlation functions showing that the pores of Braeburn apples could be modeled with spheres having an average diameter of $\sim 120\,\mu m$ (Derossi et al., 2017). Similarly, Herremans et al. (2015a) who studied the differences in aeration of apple and pear structure, measured a void equivalent spherical diameter of 100 μm for Braeburn apples. The decay of two-point probability function, $S_2(r)$, shows a damped oscillating behavior that is typical of theoretical system of interconnected particles (Smith and Torquato, 1988). Based on all these considerations, it may be quite possible to simulate the cell phase of apple tissue using grain-based model with size distributions derived from CFs (Thovert and Adler, 2011). Moreover, as reported from Derossi et al. (2017) for apples, the degree of connectivity of cell phase could be represented as an index of as how densely the cells are packed in the tissue.

Fig. 3b shows that based on CFs analysis the muffin microstructure is almost perfectly isotropic. We also observe that two-point probability and cluster functions collapse on each other. The latter indicated that
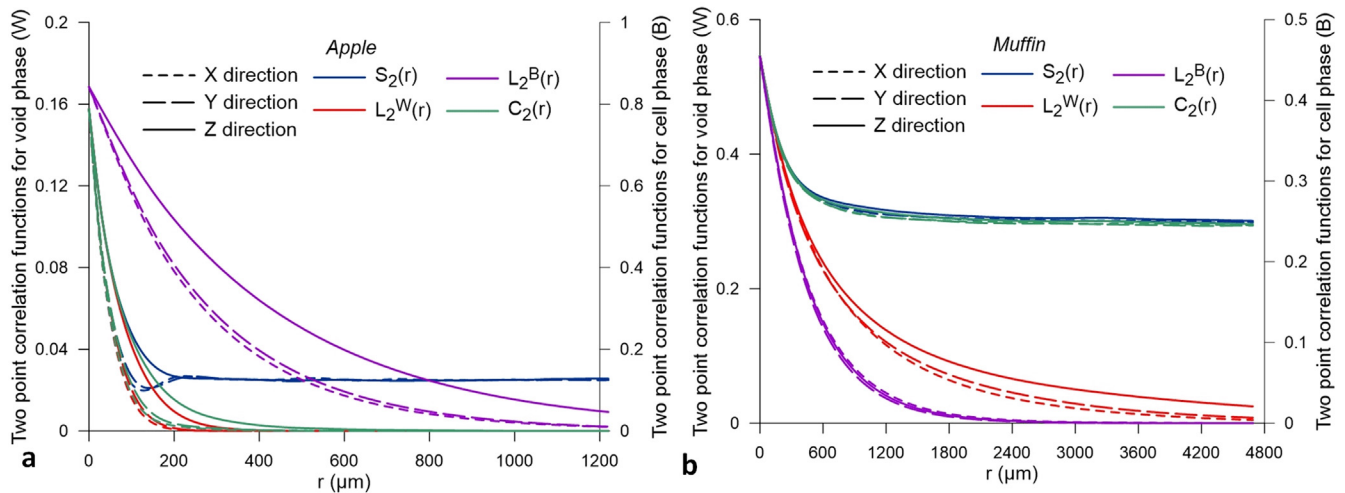
Fig. 3. All sets of correlation functions (two-point probability $S2$, linear $L2$ for both void and material (cells or solid) phases, and cluster function $C2$ for pores) computed in three major orthogonal directions for a) apple and b) muffin samples based on their whole 3D XCT images.

all pores are connected, i.e., S_2 representing the possibility that both ends of the line segment fall into the same phase also falls in the same pore cluster (C_2) all the time. The muffin's structure is characterized by pores which extend along three orthogonal directions up to 4.7 mm, although the probability to find a pore of such size drops below 0.01%. For the solid phase (i.e. the crumb) a shorter range correlation was observed which indicates that solids are mainly characterized by thin crumb elements. For instance, the probability to find a solid element of 4 mm thickness was lower than 1%. Linear functions showed values greater than the 5% only for $r < 1.62$ mm. By considering that the size length of the sample is 15.05 mm, muffin's crumb can be considered to be very thin.

The analysis of XCT images by means of correlation functions and porosity variations as shown in Fig. 2 allows to summarize some properties of apple and muffin microstructure important for their general microstructure characterization and stochastic reconstructions: 1) apple sample exhibited some degree of anisotropy in Z-direction, but we still consider it to be isotropic enough for 3D reconstructions based on 2D input image; 2) the fluctuations of porosity in Fig. 2a in the form of white noise indicate that general homogeneity of the microstructure, that is also an important requirement for CFs evaluation; 3) contrary to the apple sample, muffin shows the signs of heterogeneity - significant porosity fluctuations in Fig. 2b; approximately one third of the sample along Z-axis has porosities below average, whilst the other two thirds fluctuate above average porosity; 4) in general muffin's microstructure seems to be very isotropic, except for minor anisotropy in the solid phase, that may be the result of the aforementioned inhomogeneity.

3.2. Stochastic reconstructions and their quality

In all cases the energies fell below 10^{-9} and we can safely conclude that global energy minima were achieved. Stochastic reconstructions consisted of 512^3 voxels and it took on average approximately 0.227 s to perform 1000 permutation with i5 CPU on a regular laptop computer. With very strict annealing termination criterion described in Methods section it took on average ~5.38 days to finalize each reconstruction. Note that as was argued by Gerke et al. (2015), all reconstruction parameters and especially termination criterion (10^6 consecutive unsuccessful permutations) drastically affect computation time, thus decent accuracy of the reconstruction can be achieved within much less timeframes.

We start the comparison between original XCT images and their stochastic replicas by visually assessing the similarities between microstructures shown in Fig. 4. By first looking into 3D visualizations we

notice that apple reconstructions resemble the original XCT image closely, which is further evidenced by looking at 2D cross-section on the right hand side of the figure. For the muffin sample the comparison is not that favorable anymore. While in general we do observe somewhat similar aggregations of solid phase separating large voids, a closer look reveals notable differences in pore and crumb shapes and connectivity. More specifically, crumb agglomerates seem to be less connected and some are hanging in void phase, which is unphysical. Especially evident from 2D cross-sections, reconstructed muffin pores are less round and can be characterized as rugged or dissected. Moreover, small-sizes pores within muffin's crumb are considerably underrepresented.

To make the comparison more quantitative we now perform graphical juxtaposition of correlation functions computed for 3D XCT images and stochastic replicas. As was explained in the Methodology section, cluster function was not utilized for reconstruction and, thus, serves as a separate accuracy measure. In addition to C_2 it is actually still very useful to look at S_2 and L_2 functions, as stochastic reconstructions were performed based on CFs computed from the single 2D cross-sections. Moreover, as microstructure statistical descriptors in Z-direction were deduced as averages of these for X and Y directions it is interesting to check if this third unknown from 2D images direction was correctly represented in stochastic replicas. Note that original XCT CFs are exactly the same as on Fig. 3, but will be presented again on Figs. 5 and 6 for the ease of comparison against CFs of the reconstructed microstructures.

The CFs results for the apple sample are presented at Fig. 5. What is immediately evident for both reconstruction 1 (Fig. 5a) and reconstruction 2 (Fig. 5b), is that all CFs in Z-direction were not accurately captured by averages along X and Y axes. We recall that this difference in the Z-direction is most likely due to the sample orientation within the apple and represents the anisotropy in the radial direction on the apple's equator, which could be the result of the cell growth. This could be fixed by taking two cross-perpendicular 2D slices through the apple structure and creating target CFs set in all directions (Jiao and Chawla, 2014). The two-point probability functions for reconstructions exhibited some visible fluctuations not visible on original CFs. This is easy to explain, as all reconstructions are based on a single 2D image and, thus, represent CFs for this image. On the other hand, CFs of original XCT image are computed across full stack of 2D images (forming the 3D image), that form a much smoother curve. Such differences between 2D and full 3D sample CFs may be also seen as a measure of representability. The most surprising result came from C_2 function comparison – unlike the original apple microstructure, the pore space in both stochastic replicas percolated in all three major directions. It is
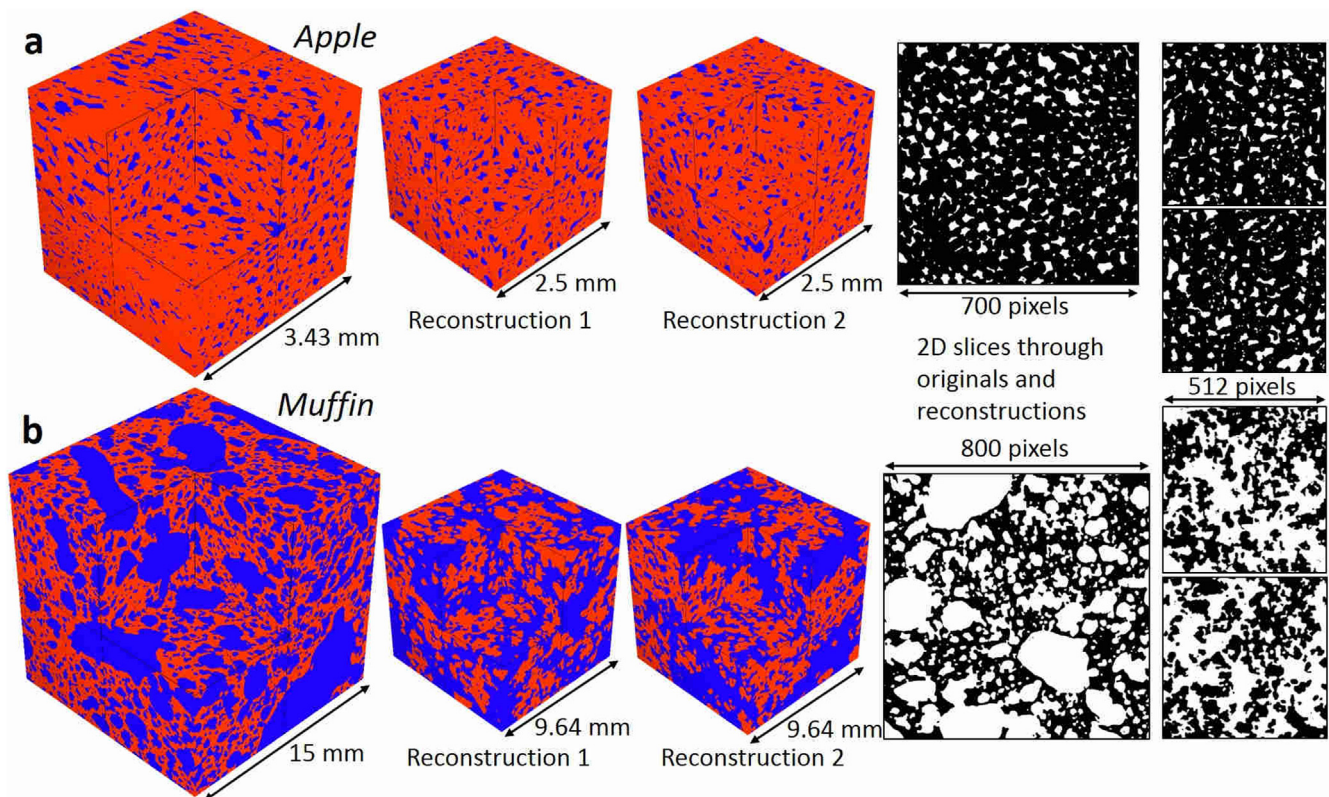
Fig. 4. Visualizations of 3D pore-solid structure for original XCT images and their stochastic replicas of a) apple and b) muffin samples. Pores are shown in blue, while solid phase is in red. The right part of the figure presents some examples of 2D cross-section through the original XCT microstructure and its stochastic reconstructions for improved visibility. Note that all 2/3D images are scaled to represent the differences in image sizes (image resolutions are the same). (For interpretation of the references to colour in this figure legend, the reader is referred to the Web version of this article.)

generally acknowledged that stochastic reconstructions based on S_2 and L_2 CFs result in lower connectivity pore geometries for low porosity structures ($\varepsilon < 30\%$), which is not the case here. Reconstruction 2 (Fig. 5b) had slightly less connected void phase than that of the Reconstruction 1 (Fig. 5a).

If we compare CFs between original XCT and reconstructions for muffin sample (Fig. 6), the agreement is actually much better than for the apple. For this reason, we have chosen to plot CFs for both of them together. All C_2 and S_2 functions agree quite well, while fluctuations are visible for these functions and can be explained in the similar manner, as it was done for the apple sample earlier. The linear functions for the crumb phase agree perfectly, whilst L_2 for the void phase show some slight degree of discrepancy, but, again, the Z-direction dominates in this respect.

The important morphological characteristics computed for original XCT and reconstructed images for both samples are reported in Table 1, while Fig. 7 shows pore-size distributions. As expected, void phase ratios agree well for all four reconstructions, as the zeroth moment of all CFs employed here immediately provides the relevant (void or solid) phase fraction. All very minor differences in porosity is only due to the differences between 2D cross-sections and 3D XCT images (Fig. 2). The total number of separate pores was higher in 3D reconstructions than in original XCT images for the apple sample. This, in turn, resulted in somewhat higher surface/volume ratios for stochastic replicas. Surface convexity index for apple microstructure was very well represented in reconstructions. Structure thickness (i.e., average pore size from inscribed spheres) is perfectly reflected according to the pore size distribution reported in Fig. 7a. The reason for very small deviations in thickness parameter and size distribution for largest pore voids (the tail of the distribution) is due to representatively issues with 2D cross-section used for reconstructions – statistical descriptors capture only the

size of the pores available on the input 2D slice, whilst original apple XCT image has larger pores within its volume. Structure separation (i.e., average apple cell size from inscribed spheres) values are significantly smaller for apple stochastic replicas, which is mainly due to a larger number of small pores scattered within the solid phase (as evident from higher number of objects). The overpredicted connectivity of the pore space discussed in Section 3.1 is also evident from the computed Err_{C_2} (Table 1).

The number of pores for the muffin was very close if compared between XCT image and stochastic replicas. Yet, the rest of the morphological characteristics suffer from considerable disagreement. The surface/volume ratio for the void phase was an order of magnitude lower on reconstructed microstructures. Moreover, convexity index for pore-solid interface was also much lower and very poorly represented by stochastic reconstructions. This can be explained from the viewpoint of the pore shapes (e.g., see 2D slices on Fig. 4) and absence of smaller pores within the crumb as discussed above. The average pore size (structure thickness) for the XCT image is two times larger than for the stochastic replicas. The absence of the smaller pores within the crumb and largest pores between the crumb agglomerates is immediately evident from the pore-size distributions (Fig. 7b). Structure separation for replicas shows somewhat higher values with a difference no more than 20%. This implies that crumb is slightly thicker compared to the original XCT muffin image. The connectivity difference error for muffin reconstructions (Table 1) is much lower compared to the apple replicas, but further inference is hampered by the presence of two porosity domains (as will be discussed in the next Section).

All in all, 3D stochastic reconstructions based on a single 2D slice worked generally well for apple microstructure, but failed to represent numerous important characteristics of both pores and crumb phases for muffin sample.
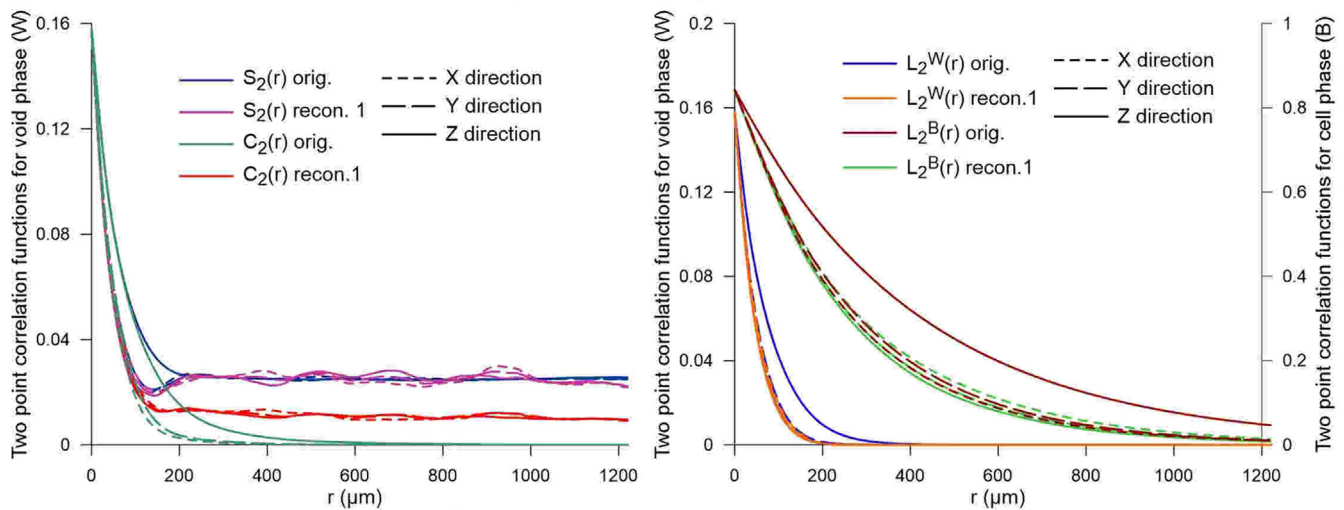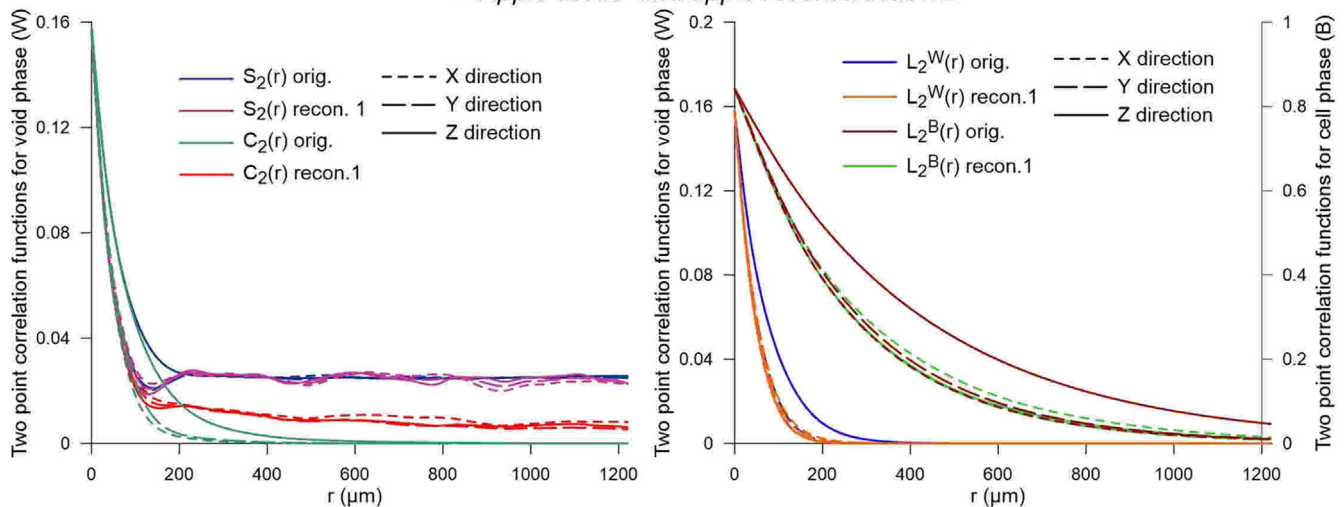
Fig. 5. Comparison between original 3D XCT images of the apple tissue and both of its reconstructions in terms of correlation functions computed in three orthogonal directions.
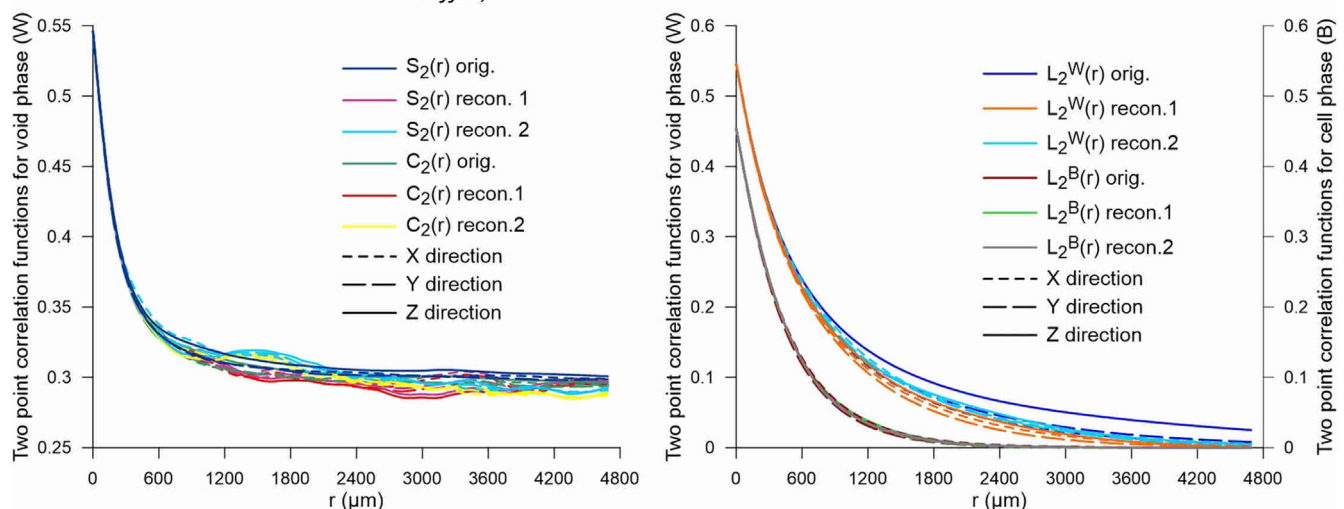
Fig. 6. Comparison between original 3D XCT images of muffin and its reconstructions in terms of correlation functions computed in three orthogonal directions.

Table 1
Main morphological characteristics of 3D microstructure of original XCT images and their stochastic reconstructions.

| Morphological properties	Apple			Muffin		
	Original XCT	Recon.1	Recon.2	Original XCT	Recon.1	Recon.2
Void fraction	15.69	15.66	15.65	54.62	54.62	54.59
Number of pores	7546	12055	17480	2025	2612	2398
Surface/volume ratio for pores	0.06982	0.08411	0.08357	0.0733	0.00785	0.00771
Surface convexity index	0.03381	0.04365	0.04392	0.00446	−0.00014	0.00019
Structure thickness	65.62	57.64	59.43	1016.04	537.67	558.344
Structure separation	160.67	118.48	118.17	314.25	367.99	370.11
Connectedness difference Err_{C_2}	0	0.02857521	0.02047631	0	0.00686339	0.01123981

3.3. General discussion and outlook

The main question that arises after analysis of all results presented above is – what was the reason for some aspects of microstructure to be represented perfectly by stochastic reconstructions, especially for apple sample, while many characteristics of the muffin sample were represented poorly? Based on all results and detailed analysis presented above we believe that there are three main reasons for this to happen: 1) insufficient representability of the input 2D cross-sections used to compute target CFs sets; 2) statistical inhomogeneity of the structures under study (for muffin samples); and 3) insufficiency of two-point probability and linear correlation functions to fully describe food microstructure. Clear explanation of all of these issues requires more elaboration.

If we consider again the porosity variations within 2D slices shown in Fig. 2, for apple we observe some steady fluctuations around the average porosity value. Both representative slices we chose to reconstruct apple's microstructure not only matched the average porosity, they also had CFs very close to that of the whole 3D image of original apple tissue structure (Fig. 5a), which in turn ensured that CFs (except for C_2 function) for 3D stochastic replica will match XCT image very closely. It is also important to clarify in this context, that as both 2D slices provided directly only CFs in X and Y-directions, here we mean the agreement in these two directions. Pore sizes are quite evenly distributed within the apple sample (as visible on Fig. 4a), thus, all pore sizes and shapes are present on the input 2D images. This, in turn, ensured that reconstructed 3D images had pore size distributions that matched the original XCT image closely (Fig. 7a). In short, for apple the chosen 2D slices were representative not only in terms of porosity, but also in terms of microstructure – CFs, pore sizes and shapes. Yet, we observe on Fig. 4a that original apple microstructure includes both evenly porous regions, which are nicely reproduced on stochastic replicas, and sparsely porous regions not present on reconstructions. This implies that apple structure is not strictly statistically homogeneous, and such porosity non-stationarities were not sampled by representative 2D slices. More even porosity distribution on the reconstructed images can partially explain why replicas turned out to be more connected than XCT microstructure. This is evident on the right side of the Fig. 4a where very similar porosity distributions on original and reconstructed 2D images are apparent. As was pointed out previously by Karsanina et al. (2015) – while image homogeneity is assumed in conventional reconstruction techniques, it is never rigorously confirmed numerically. Moreover, one could expect that majority of natural microstructures (food, rocks, soils and such) are never strictly statistically homogeneous. If stochastic reconstructions were produced from CFs computed from the whole 3D XCT image, we expect that such minor inhomogeneities would be reproduced by our methodology, but this requires confirmation in the future research.

The muffin case is more complex – from the porosity analysis on Fig. 2b and visual porosity distribution (see Fig. 4b) we infer that all aforementioned reasons had their place for this sample. Porosity variation within 2D slices along Z-direction indicates that one third of the sample has porosity below average (the upper part on Fig. 4b), whilst due to the presence of the large pores in lower part of the 3D microstructure other two thirds have higher than average porosity. Both 2D slices chosen as input images are unlikely to be representative, as they were taken from the transition zone between these two low and high porosity domains. This conclusion is partially supported by pore size distribution (Fig. 7b) and morphological characteristics (Table 1) disagreement. Another factor – statistical inhomogeneity of the muffin microstructure - is actually a two-fold problem. Not only there is an inhomogeneity in terms of porosity variations in 2D slices, but another
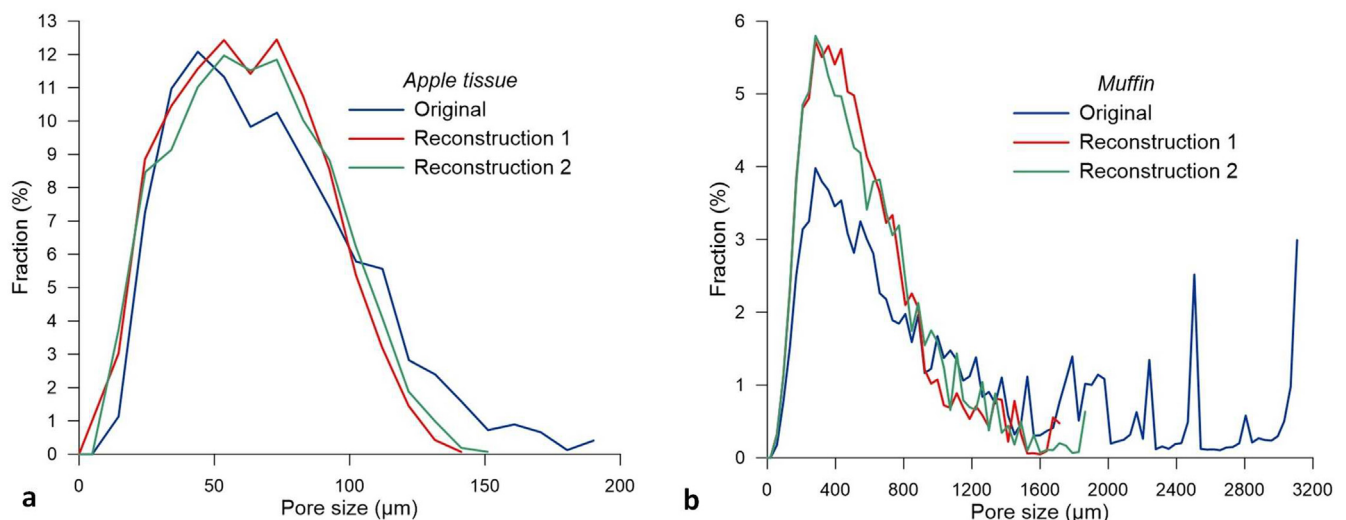
Fig. 7. Pore-size distributions within original XCT images of a) apple and b) muffin and their stochastically reconstructed counterparts.

non-stationarity is clearly observed within separate slices: smaller and somewhat isolated pores are present within the crumb, while larger and highly connected pores separate crumb agglomerates. These two distinct porosity domains have different microstructure and, thus, reconstructions based on ensemble averaged directional CFs show only very limited distinctions between them. It is worth to note that it is not possible to separate stochastic reconstruction inaccuracies resulting from 2D slice non-representability and non-stationarity of the original microstructure. Interestingly, although CFs, including cluster function C_2, for original muffin XCT image and reconstructions (Fig. 6) agree closely, due to non-stationarity issues this does not guarantee accurate stochastic replication. Unlike for the apple microstructure, we do not expect that performing reconstruction based on original XCT image would improve the quality of the replicas significantly. Thus, statistical inhomogeneity poses an important problem that requires its solution for food engineering applications.

After we have identified the reasons for stochastic reconstruction inaccuracies in case of apple and muffin microstructure, the next question is if we can prevent them and how? To address non-representability issue, a number of solutions could be utilized such as: to utilize a larger field-of-view 2D image that includes all pores sizes and porosity zones or to reconstruct from more than one 2D slices (e.g., Karsanina et al., 2018). In the latter case the usage of cross-perpendicular cuts would also address the problem with slight *Z*-direction anisotropy experienced in this work, or even allowed to reconstruct anisotropic microstructures. Using, for example, *Y-Z* averaging instead of taking slices along *Z*-direction would not improve the results obtained in this work significantly and, thus, was not attempted. It seems always more beneficial to perform reconstruction from 3D images, but using a limited structural information as input data is useful in many instances, especially then 3D imaging is not readily available. There are also plenty of options for addressing the statistical inhomogeneity issue. Variation of porosity along *Z*-direction (as in muffin sample) or presence of the loose porosity subvolumes (as in the apple microstructure) can be fixed by separate reconstruction of statistically homogeneous portions of the image (Tahmasebi and Sahimi, 2015). The case of different porosity domains within and in-between muffin crumb can be effectively addressed by their separate reconstruction with subsequent fusion (Gerke et al., 2015; Karsanina et al., 2018). Karsanina et al. (2015) extensively discussed the problem of inability to describe any structure at hand by S_2 and L_2 CFs using the concept of information content developed by Gommes et al. (2012). This problem is probably the hardest to address, but in general it is possible to increase the number of correlation functions (Torquato, 2002) employed for reconstruction until stochastic replicas will represent the original with desired accuracy. This paragraph is more of the outlook, but while all proposed solutions are beyond the scope of this work and will be explored in the future, it is important to highlight that solutions are available, yet require adaptation for food engineering research.

4. Conclusions

We have presented the first results on the capability to mimic 3D structure of food specimens, apple tissue and muffin, by reconstructing their microstructure using limited statistical information from single 2D images. In short, lineal-path and two-point probability functions were employed as input data to test the capability to create replicas of the food. In the case of apple tissue the reconstructions matched the original 3D image well, although we have revealed a slight degree of anisotropy in the direction not captured by the input 2D slice. For muffin, previously developed conventional approaches showed very limited accuracy due to insufficient representability of the input 2D image(s) and due to the structural complexity consisting of at least two different porosity domains. Novel stochastic reconstruction and CF-based characterization methods should be specifically developed or adapted in the future to improve the fidelity of 3D reconstruction.

Current results have opened the way of mimicking food microstructure and have the potential to provide robust tools for estimation of the essential macroscopic properties of food based on limited 2D information.

Author contributions

A.D. conceived and coordinated this study; K.M.G. and M.V.K. designed and performed all methodological procedures; M.V.K. developed stochastic reconstruction codes; K.M.G. and A.D. drafted the major part of the manuscript; M.V.K. and K.M.G. prepared graphical materials; A.D. and P.V. performed and analyzed X-ray microtomography images, P.V., B.N. and C.S. helped in interpreting results; all authors reviewed the final version of the paper.

References

Abera, M.K., Verboven, P., Herremans, E., Defraeye, T., Fanta, S.W., Ho, Q.T., Carmeliet, J., Nicolai, B., 2014. 3D Virtual Pome fruit tissue generation based on cell growth modeling. Food Bioprocess Technol. 2, 542–555.

Adler, P.M., Jacquin, C.G., Quiblier, J.A., 1990. Flow in simulated porous media. Int. J. Multiphas. Flow 16 (4), 691–712.

Aguilera, J.M., 2005. Why food microstructure? J. Food Eng. 67, 3–11.

Buades, A., Coll, B., Morel, J.M., 2005. A non-local algorithm for image denoising. In Computer Vision and Pattern Recognition, 2005. CVPR 2005. In: Proceeding of IEEE Computer Society Conference. vol. 2. pp. 60–65.

Capek, P., Hejtmanek, V., Brabec, L., Zikanova, A., Kocirik, M., 2009. Stochastic reconstruction of particulate media using simulated annealing: improving pore connectivity. Transport Porous Media 76, 179–198.

Čapek, P., Hejtmánek, V., Kolafa, J., Brabec, L., 2011. Transport properties of stochastically reconstructed porous media with improved pore connectivity. Transport Porous Media 88 (1), 87–106.

Chan, T.P., Govindaraju, R.S., 2004. Estimating soil water retention curve from particle-size distribution data based on polydisperse sphere systems. Vadose Zone J. 3, 1443–1454.

Coker, D.A., Torquato, S., Dunsmuir, J.H., 1996. Morphology and physical properties of Fontainebleau sandstone via a tomographyc analysis. J. Geophys. Res.: Solid Earth 101, 17497–17506.

Datta, A.K., 2007. Porous media approaches to studying simultaneous heat and mass transfer in food processes. I: problem formulations. J. Food Eng. 80, 80–95.

Derossi, A., De Pilli, T., Severini, C., 2013. Statistical Description of Food Microstructure. Extraction of some correlation functions from 2D images. Food Biophys. 8, 311–320. https://doi.org/10.1007/s11483-013-9307-2.

Derossi, A., Severini, C., De Pilli, T., 2014. Reconstruction of food microstructure via statistical correlation functions. The use of lineal-path distribution functions. J. Food Eng. 142, 9–16. https://doi.org/10.1016/j.jfoodeng.2014.05.020.

Derossi, A., Nicolai, B., Verboven, P., Severini, C., 2017. Characterizing apple microstructure via directional statistical correlation functions. Comput. Electron. Agric. 138, 157–166. https://doi.org/10.1016/j.compag.2017.04.021.

Derossi, A., Severini, C., Ricci, I., 2016. On the inverse problem of the reconstruction of food microstructure from limited statistical information. J. Food Eng. 184, 69–74. https://doi.org/10.1016/j.jfoodeng.2016.03.025.

Gerke, K.M., Karsanina, M.V., 2015. Improving stochastic reconstructions by weighting correlation functions in an objective function. EPL Europhysics letters 111, 56002. https://doi.org/10.1209/0295-5075/111/56002.

Gerke, K.M., Karsanina, M.V., Mallants, D., 2015. Universal stochastic multi-scale image fusion: an example application for shale rock. Sci. Rep. 5, 15880. https://doi.org/10.1038/srep15880.

Gerke, K.M., Karsanina, M.V., Skvortsova, E.B., 2012. Description and reconstruction of the soil pore space using correlation functions. Eurasian Soil Sci. 45 (9), 962–973.

Gerke, K.M., Karsanina, M.V., Sizonenko, T.O., Miao, X., Gafurova, D.R., Korost, D.V., 2017. Multi-scale image fusion of X-ray microtomography and SEM data to model flow and transport properties for complex rocks on pore-level. In: SPE 187874 Technical Paper, Presented at SPE Russian Petroleum Technology Conference, 16-18 October, Moscow, Russia, https://doi.org/10.2118/187874-MS.

Gerke, K.M., Karsanina, M.V., Vasilyev, R., Mallants, D., 2014. Improving pattern reconstruction using directional correlation functions. Europhysics Letters, EPL 106 (66002), 1–6. https://doi.org/10.1209/0295-5075/106/66002.

Gommes, C.J., Jiao, Y., Torquato, S., 2012. Microstructural degeneracy associated with a two-point correlation function and its information content. Phys. Rev. 85 (5),

051140.

Guo, E.Y., Chawla, N., Jing, T., Torquato, S., Jiao, Y., 2014. Accurate modeling and re-construction of three-dimensional percolating filamentary microstructure from two-dimensional micrographs via dilation-erosion method. Mater. Char. 89, 33–42.

Hafsa, I., Cuq, B., Kim, S.J., Le Bail, A., Ruiz, T., Chevallier, S., 2014. Description of internal microstructure of agglomerated cereal powders using X-ray micro-tomography to study of process-structure relationships. Powder Technol. 256, 512–521.

Herremans, E., Verboven, P., Defraye, T., Rogge, S., Ho, Q.T., Hertog, L.A.T.M., Verlinden, B.E., Bongaers, E., Wevers, M., Nicolai, B.M., 2014. X-ray CT for quanti-tative food microstructure engineering: the apple case. Nucl. Instrum. Methods Phys. Res., Sect. B 324, 88–94.

Herremans, E., Verboven, P., Verlinden, B.E., Cantre, D., Abera, M., Weverss, M., Nicolai, B.M., 2015a. Automatic analysis of the 3-D microstructure of fruit parenchyma tissue using X-ray micro-CT explains difference in aeration. BMC Plant Biol. 15, 264.

Herremans, E., Verboven, P., Hertog, M.L.A.T.M., Cantre, D., van Dael, M., De Schryver, T., Van Hoorebekem, L., Nicolai, B.M., 2015b. Spatial development of transport structures in apple (Malus x domestica Borkh.) fruit. Front. Plant Sci. https://doi.org/10.3389/fpls.2015.00679.

Jiao, Y., Chawla, N., 2014. Modeling and characterizing anisotropic inclusion orientation in heterogeneous material via directional cluster functions and stochastic micro-structure reconstruction. J. Appl. Phys. 115, 093511.

Jiao, Y., Stillinger, F.H., Torquato, S., 2009. A superior descriptor of random textures and its predictive capacity. PNAS – Proc. Nat. Acad. Sci. United States of America 106 (42), 17634–17639.

Karsanina, M.V., Gerke, K.M., Skvortsova, E., Mallants, D., 2015. Universal spatial cor-relation functions for describing and reconstructing soil microstructure. PLoS One 10, 1–26. https://doi.org/10.1371/journal.pone.0126515.

Karsanina, M.V., Gerke, K.M., Skvortsova, E.B., Ivanov, A.L., Mallants, D., 2018. Enhancing image resolution of soils by stochastic multiscale image fusion. Geoderma 314, 138–145. https://doi.org/10.1016/j.geoderma.2017.10.055.

Kirkpatrick, S., Gelatt, C.D., Vecchi, M.P., 1983. Optimization by simulated annealing. Science 220 (4598), 671–680.

Kumar, H., Briant, C.L., Curtin, W.A., 2006. Using microstructure reconstruction to model mechanical behavior in complex microstructures. Mech. Mater. 38, 818–832.

Lee, S.B., Torquato, S., 1988. Pair connectedness and mean cluster size for continuum-percolation models – computer-simulation results. J. Chem. Phys. 89 (10), 6427–6433.

Li, H., Singh, S., Kaira, S., Mertens, J.C.E., Williams, J.J., Chawla, N., Jiao, Y., 2016. Microstructural quantification and property prediction using limited X-ray tomo-graphy data. J. Miner. Met. Mater. Soc. 68 (8), 2288–2295.

Lu, B., Torquato, S., 1992. Lineal-path function for random heterogeneous materials II. Effects of polydispersivity. Phys. Rev. 45 (10), 7292–7301.

Manwart, C., Torquato, S., Hilfer, R., 2000. Stochastic reconstruction of sandstone. Phys. Rev. 62 (1), 893.

Metropolis, N., Rosenbluth, A.W., Rosenbluth, M.N., Teller, A.H., Teller, E., 1953. Equation of state calculations by fast computing machines. J. Chem. Phys. 21 (6), 1087–1092.

Miao, X., Gerke, K.M., Sizonenko, T.O., 2017. A new way to parameterize hydraulic conductances of pore elements: a step towards creating pore-networks without pore shape simplifications. Adv. Water Resour. 105, 162–172.

Parada, J., Aguilera, J.M., 2007. Food microstructure affects the bioavailavility of several nutrients. J. Food Sci. 72 (2), 21–32.

Quiblier, J.A., 1984. A new-three dimensional modeling technique for studying porous media. J. Colloid Interface Sci. 98 (1), 84–102.

Reinke, S.K., Wilde, F., Kozhar, S., Beckmann, F., Vieria, J., Heinrich, S., Palzer, S., 2016. Synchrotron X-ray microtomography reveals interior microstructure of multi-component food materials such as chocolate. J. Food Eng. 174, 37–46.

Rintoul, M.D., Torquato, S., 1997. Reconstruction of the structure of dispersions. J. Colloid Interface Sci. 186, 467.

Rintoul, M.D., Torquato, S., Yeong, C., Keana, D.T., Eramilli, S., Jun, Y.N., Dabbs, D.M., Aksay, I.A., 1996a. Structure and transport properties of a porous magnetic gel via X-ray microtomography. Phys. Rev. 54 (3), 2663–2669.

Rintoul, M.D., Torquato, S., Yeong, C., Keane, D.T., Erramilli, S., Jun, Y.N., 1996b. Structure and transport properties of porous magnetic gel via x-ray micro-tomography. Phys. Rev. 54 (3), 2663–2669.

Rozman, M.G., Utz, M., 2002. Uniqueness of reconstruction of multiphase morphologies from two-point correlation functions. Phys. Rev. Lett. 89 (13). https://doi.org/10.1103/PhysRevLett.89.135501. 135501.

Severini, C., Derossi, A., Ricci, I., Caporizzi, R., Fiore, A., 2017. In: New Advances in Spent Coffee Valorization. A More Sustainable Reuse as Whole Ingredients to Develop Nutritionally Enriched Muffins. 31st Effost International Conference, 13-16 November, Sitges, Spain.

Sheidaei, A., Baniassadi, M., Banu, M., Askeland, P., Pahlavanpour, M., Kuuttila, N., Pourboghrat, F., Drzal, L.T., Garmestani, H., 2013. 3-D microstructure reconstruction of polymer nano-composite using FIB-SEm and statistical correlation function. Compos. Sci. Technol. 80, 47–54.

Sheppard, A.P., Sok, R.M., Averdunk, H., 2004. Techniques for image enhancement and segmentation of tomographic images of porous materials. Phys. Stat. Mech. Appl. 339 (1–2), 145–151.

Smith, P., Torquato, S., 1988. Computer simulation results for the two-point probability function of composite media. J. Comput. Phys. 76, 176–191.

Tahmasebi, P., Sahimi, M., 2015. Reconstruction of nonstationary disordered materials and media: watershed transform and cross-correlation function. Phys. Rev. 91 (3), 032401.

Takhar, P.S., 2016. Incororating food microstructure and material characteristics for developing multiscale saturated and unsaturated transport models. Current Opinion in Food Science 9, 104–111.

Talukdar, J.J., Torsaeter, O., Ioannidis, M.A., Howard, J.J., 2002. Stochastic re-construction, 3D characterization and network modeling of chalk. J. Petrol. Sci. Eng. 35 (1–2), 1–21.

Thovert, J.F., Adler, P.M., 2011. Grain reconstruction of porous media: application to a Bentheim sandstone. Phys. Rev. 83 (5), 056116.

Torquato, S., 2002. Random Heterogeneous Materials: Microstructure and Macrostructure Properties. Springer-Verlag, New York 2002.

Torquato, S., Lu, B., 1993. Chord-length distribution function for two-phase random media. Phys. Rev. 47 (4), 2950–2953.

Van Dyck, T., Verboven, P., Herremans, E., Defraye, T., van Capenhout, L., Wevers, M., Claes, J.E., Nicolai, B., 2014. Characterisation of structural patterns in bread as evaluated by X-ray computer tomography. J. Food Eng. 123, 67–77.

Verboven, P., Defraeye, T., Nicolai, B., 2018. Measurement and visualization of food microstructure: fundamentals and recent advances. In: Food Microstructure and its Relationships with Quality and Stability. Woodhead Publishing, pp. 3–28.

Verboven, P., Nemeth, A., Abera, M.K., Bongaers, E., Daelemans, D., Estrade, P., Herremans, E., Hertog, M., Saeys, W., Vanstreels, E., Verlinden, B., Leitner, M., Nicolai, B., 2013. Optical Coherence tomography visualizes microstructure of apple peel. Postharvest Biol. Technol. 78, 123–132.

Verboven, P., Kerckhofs, G., Mabation, H.K., Ho, Q.T., Temsts, K., Wevers, M., Cloetens, P., Nicolai, B.M., 2008. Three-dimensional gas exchange pathways in pome fruit characterized by synchrotron X-ray computed tomography. Plant Physiol. 147, 518–527.

Vesely, M., Bultreys, T., Peksa, M., Lang, J., Cnudde, V., van Hoorebeke, L., Kocirik, M., Hejtmanek, V., Solcova, O., Soukup, K., Gerke, K.M., Stallmach, F., Capek, P., 2015. Prediction and evaluation of time-dependent effective self-diffusivity of water and other effective transport properties associated with reconstructed solids. Transport Porous Media 110 (1), 81–111.

Yao, J., Frykman, P., Kalaydjian, F., Thovert, J.F., Adler, P.M., 1993. High-order moments of the phase function for real and reconstructed model porous media: a comparison. J. Colloid Interface Sci. 156 (2), 478–490.

Yeong, C.L.Y., Torquato, S., 1998a. Reconstructing random media. Phys. Rev. E 57 (1), 495.

Yeong, C.L.Y., Torquato, S., 1998b. Reconstructing random media II. Three dimensional media from two-dimensional cuts. Phys. Rev. E 58 (1), 224.

Yin, P., Zhao, G.F., 2014. Stochastic reconstruction of Gosford sandstone from surface image. Int. J. Rock Mech. Miming Sci. 70, 82–89.